Strongly correlated systems in atomic and condensed matter physics

Lecture notes for Physics 284

by Eugene Demler

Harvard University

January 29, 2018

Chapter 4

Spinor condensates

4.1 Two component mixtures

We consider two species of bosons. This may be two hyperfine states of the same atom or two different species.

$$\begin{aligned}\mathcal{H} &= \frac{1}{2m_1}\int d^3r\,|\nabla\Psi_1|^2 + \frac{1}{2m_2}\int d^3r\,|\nabla\Psi_2|^2 \\ &+ \frac{U_{11}}{2}\int d^3r\,\Psi_1^\dagger\Psi_1^\dagger\Psi_1\Psi_1 + U_{12}\int d^3r\,\Psi_1^\dagger\Psi_2^\dagger\Psi_2\Psi_1 + \frac{U_{22}}{2}\int d^3r\,\Psi_2^\dagger\Psi_2^\dagger\Psi_2\Psi_2 \\ &- \mu_1\int d^3r\,\Psi_1^\dagger\Psi_1 - \mu_2\int d^3r\,\Psi_2^\dagger\Psi_2 \end{aligned} \tag{4.1}$$

In this section we assume that all interactions are repulsive, $U_{ij} > 0$.

Mean-field energy for a state with two condensates is given by

$$\frac{E}{V} = \frac{U_{11}}{2}|\Psi_1|^4 + U_{12}|\Psi_1|^2|\Psi_2|^2 + \frac{U_{22}}{2}|\Psi_2|^4 - \mu_1|\Psi_1|^2 - \mu_2|\Psi_2|^2 \tag{4.2}$$

To find the phase diagram we need to minimize this energy functional with respect to $|\Psi_1|$ and $|\Psi_2|$ at given chemical potentials. We can have two types of phase diagrams. In the case $U_{11}U_{22} > U_{12}^2$ we have a miscible system (see fig 4.1). In this case we find a uniform mixed phase with finite density of both types of atoms. As one varies chemical potentials, densities change continuously.

In the case $U_{11}U_{22} < U_{12}^2$ we have an immiscible system. In the phase diagram with chemical potentials as tuning parameters there is a direct first order transition line between condensates of species one and species two (see fig 4.2). Densities change discontinuously across this transition line. However when one controls densities rather than chemical potentials, one can prepare a system with finite density of both species. Thermodynamic equilibrium in this case corresponds to the phase separated regime.

In the case of ultracold atoms one can also explore intersting questions regarding dynamics of phase separation. For example, it is possible to prepare

a mixture of ultracold atoms in the immiscible regime dynamically. When two species correspond to two hyperfine states of the same atom, one can start with a BEC in one of the hyperfine states, then do the so-called $\pi/2$ rotation. Such rotation takes each atom into a coherent superposition of being in state 1 and 2. So the initial state has $\langle\Psi_1\rangle = \langle\Psi_2\rangle = \Psi_0$. However, such state is not an equilibrium state and is therefore unstable. A good understanding of how the instability develops can be obtained from analyzing collective modes.

Two component GP equations in this case can be written as

$$\begin{aligned} i\frac{\partial\Psi_1}{\partial t} &= -\frac{\nabla^2}{2m}\Psi_1 + U_{11}|\Psi_1|^2\Psi_1 + U_{12}|\Psi_2|^2\Psi_1 - \mu_1\Psi_1 \\ i\frac{\partial\Psi_2}{\partial t} &= -\frac{\nabla^2}{2m}\Psi_2 + U_{12}|\Psi_1|^2\Psi_2 + U_{22}|\Psi_2|^2\Psi_2 - \mu_2\Psi_2 \end{aligned} \tag{4.3}$$

This is a non-equilibrium problem. Hence we can not think of the chemical potential terms as imposing certain densities. We set the chemical potentials by requiring that $\langle\Psi_1\rangle = \langle\Psi_2\rangle = \Psi_0$ satisfies a stationary solution $\dot{\Psi}_i = 0$.

$$\begin{aligned} \mu_1 &= (\,U_{11} + U_{12}\,)\,n_0 \\ \mu_2 &= (\,U_{12} + U_{22}\,)\,n_0 \end{aligned} \tag{4.4}$$

where $n_0 = |\Psi_0|^2$. Equations (4.4) are equivalent to saying that in the canonical ensemble, which is more appropriate for this nonequilibrium problem, $\Psi_{\{1,2\}\,\mathrm{canonical}}(t) = \Psi_0 e^{-i\mu_{\{1,2\}}t}$.

We now consider small deviations from the initial state, $\Psi_i = \Psi_0 + \delta\Psi_i(r,t)$ and derive linearized GP equations

$$\begin{aligned} i\delta\dot{\Psi}_1 &= -\frac{\nabla^2}{2m}\delta\Psi_1 + U_{11}n_0(\delta\Psi_1 + \delta\Psi_1^*) + U_{12}n_0(\delta\Psi_2 + \delta\Psi_2^*) \\ \delta\dot{\Psi}_2 &= -\frac{\nabla^2}{2m}\delta\Psi_2 + U_{12}n_0(\delta\Psi_1 + \delta\Psi_1^*) + U_{22}n_0(\delta\Psi_2 + \delta\Psi_2^*) \end{aligned} \tag{4.5}$$

Following similar steps to the ones we used in obtaining the Bogoliubov spectrum in Chapter 3, we find that the collective mode dispersion, resulting from equations (4.5), satisfies an equation

$$(\,\omega_q^2 - \frac{q^4}{4m^2} - \frac{U_{11}n_0}{m}q^2\,)(\,\omega_q^2 - \frac{q^4}{4m^2} - \frac{U_{22}n_0}{m}q^2\,) - (\frac{U_{12}n_0}{m}q^2)^2 = 0 \tag{4.6}$$

When $U_{12}^2 > U_{11}U_{22}$, we find solutions with negative imaginary frequencies (note that this is the same criterion as immiscibility in equilibrium systems). Such imaginary solutions signal instability: small initial fluctuations grow exponentially in time. The plot of frequencies vs momentum is shown in fig 4.3. The unstable modes start at $q = 0$ and extend over a finite range of wavevectors. Vanishing of the instability rate as $q \to 0$ is a reflection of the spin conservation in the system: $N_1 - N_2$ commutes with the Hamiltonian (4.1). For large wavevectors collective modes become stable again, since having short distance modulation would cost too much kinetic energy. The growth rate of unstable

modes is maximal for some finite wavevector q_*. One expects that instabilities at this wavevector dominate so the system develops domains with the lengthscale $2\pi/q_*$.

Experiments studying domain formation in an immiscible mixture of two spin components of Na have been preformed by Miesener et al.[4, 20] (see fig.4.4). Experimentally observed domain sizes are in agreement with the theoretical analysis above[15, 20].

The problem of domain formation in immiscible two component mixtures is an example of of extending Bogoliubov analysis to study problems involving non-equilibrium dynamics. Other problems where similar formalism has been applied to analyze experiments experiments include sudden changes in the scattering length, dynamics of spinor conensates with dipolar interactions, RF slicing of one dimensional condensates.

4.2 $F = 1$ spinor condensates

4.2.1 Microscopic Hamiltonian

In this section we consider spinor condensates in optical far-off-resonant traps, which confine atoms regardless of their hyperfine state.

An $F = 1$ spinor condensate is described by a three component order parameter

$$\vec{\Psi} = \begin{pmatrix} \Psi_1 \\ \Psi_0 \\ \Psi_{-1} \end{pmatrix} \tag{4.7}$$

When there is only contact s-wave interaction between atoms (this is again an effective interaction appropriate for the low energy limit), it can be written as

$$V_{\rm int} = (V_0 P_{f=0} + V_2 P_{f=2})\delta(\vec{r}_1 - \vec{r}_2) \tag{4.8}$$

Here P_f are projection operators for the total spin of the pair of atoms, $V_f = 4\pi\hbar^2 a_f/m$, and a_f are the appropriate scattering lengths. Two identical $F = 1$ bosons can scatter with $f = 0$ or $f = 2$. Scattering with $f = 1$ is not possible because the wavefunction of the pair is antisymmetric in both spin and orbital parts.

For two $F = 1$ atoms there is an identity $\vec{F}_1 \vec{F}_2 = P_2 - 2P_0$. With the help of this identity the interaction potential can also be written as

$$\begin{aligned} V_{\rm int} &= (g_0 + g_s \vec{F}_1 \vec{F}_2)\delta(\vec{r}_1 - \vec{r}_2) \\ g_0 &= \frac{4\pi\hbar^2}{3m}(2a_{f=2} + a_{f=0}) \\ g_s &= \frac{4\pi\hbar^2}{3m}(a_{f=2} - a_{f=0}) \end{aligned} \tag{4.9}$$

The spin part of this interaction is called antiferromagnetic when $g_s > 0$ and ferromagnetic when $g_s < 0$. $F = 1$ hyperfine state of ^{23}Na atoms has antiferromagnetic interactions, and $F = 1$ hyperfine state of ^{87}Rb atoms has ferromagnetic interactions.

We can write the Hamiltonian of the system as

$$\begin{aligned} \mathcal{H} &= \int dr \,(\frac{\hbar^2}{2m}|\nabla\Psi_a|^2 - p\Psi_a^\dagger F_{ab}^z \Psi_b + q\Psi_a^\dagger (F^z)_{ab}^2 \Psi_b \\ &+ \frac{g_0}{2}\Psi_a^\dagger \Psi_{a'}^\dagger \Psi_{a'}\Psi_a + \frac{g_2}{2}\Psi_a^\dagger \vec{F}_{ab}\vec{F}_{a'b'}\Psi_{a'}^\dagger \Psi_{b'}\Psi_b) \end{aligned} \tag{4.10}$$

Here $\vec{F}_{ab}$ are spin operators. In the basis of Zeeman eigenstates which we use, $F_{ab}^z = a\delta_{ab}$ and $(F^z)_{ab}^2 = a^2\delta_{ab}$. z-component of magnetization is a conserved quantity of this Hamiltonian (it commutes with the hamiltonian) so when constructing phase diagrams, p should be thought of as a Lagrange multiplier which controls F^z. However, when one deals with spatially inhomegneous systems, in which magnetic field varies in space, one needs to recall that $p(r) = g\mu_b H(r)$. The origin of the quadratic Zeeman effect is that magnetic field primarily couples to an electron spin, whereas we describe states using hyperfine spins, which are mixtures of electron and nuclear spins, mixed by the hyperfine interaction (recall discussion of atomic states in chapter **??**). Quadratic Zeeman effect causes the energy of $m_F = 0$ state to be lower than the energy of $m_F = \pm 1$ atoms (more accurately, the energy of two $m_F = 0$ atoms is lower than the energy of $m_F = +1$ and $m_F = -1$ pair). For ^{87}Rb and ^{23}Na $q = \tilde{q}H^2$ where $\tilde{q} = h390$ Hz/G^2. Somewhat surprisingly we find that magnetic field is primarily used to control the strength of quadratic Zeeman coefficient whereas the linear Zeeman term should be thought of as determined by the prepared magnetization of the system. It is also worth noting that it is possible to create effective negative Zeeman coefficient using an AC Stark effect.

We assume that all atoms are condensed into the same state and consider mean-field energy

$$E_{\text{spin}} = -pF_z + q\langle (F^z)^2\rangle + g_2\langle \vec{F}\rangle^2 \tag{4.11}$$

The first term comes from the linear Zeeman effect. The second term in (4.11) comes from the quadratic Zeeman term. The last term in (4.11) comes from spin dependent part of the interactions.

The antiferromagnetic interaction $g_s > 0$ favors nematic (polar) state: $|m_F = 0\rangle$ or its rotations. Atoms in such state do not have expectation values of any of the spin component $\langle \vec{F}\rangle = 0$. However spin symmetry is broken (by selecting eigenstates with zero eigenvalue some direction in spin space). Such state can be characterized by the nematic order parameter

$$Q_{ab} = \frac{1}{2}(F_aF_b + F_bF_a) - \frac{1}{3}\delta_{ab}F^2 \tag{4.12}$$

which breaks spin rotational symmetry but not time reversal symmetry.

4.2.2 Mean-field phase diagram

Non-interacting case

We start by considering the case of no spin interactions. In this case we have level crossings determined by single particle states. For large positive p the system favors $m_F = +1$ state, for large q the system favors $m_F = 0$ and there is a first order transition line between the two. Analogously there s a transition between $m_F = -1$ and $m_F = 0$ states for negative p. This phase diagram is shown in fig. 4.5.

Ferromagnetic case

The ferromagnetic interaction $g_s < 0$ favors spin polarized state: $|m_F = +1\rangle$ or its rotations. In this case we no longer have direct transitions between different eigenstates of F_z, but there is an intermediate region that has a mixture of all three states. Such mixture allows to lower the interaction energy by developing a transverse spin magnetization (in the xy plane) even when it is not favorable to have large longitudinal polarization (along the z-axis). Transitions between all phases are continuous second order transitions. Phase diagram of ferromagnetic spinor condensates is shown in fig. 4.6.

Antiferromagnetic case

Antiferromagnetic interactions favor a system to become an eigenstate of $\vec{n}\vec{F}$ operator with eigenvalue zero for any direction of the vector n, which we can refer to as direction of the nematic order (we call it nematic because n and $-n$ are the same). The first effect of such interaction is to favor $m_F = 0$ state, which is already favored by the quadratic Zeeman term. A more subtle effect of antiferromagnetic interactions is to stabilize a mixed phase for small values of p and q, which has a mixture of $+1$ and -1 states. This phase has nematic order in the xy plane and helps to lower the interaction energy. Phase diagram of nematic spinor condensates is shown in fig. 4.7. Note that there is still a direct first order transition between $m_F = 0$ and $m_F = \pm 1$ states for large quadratic Zeeman shifts.

4.2.3 Exeriments with $F = 1$ spinor condensates

Experiments verifying the phase diagram of spinor condensate with AF interactions have been done by Stenger et al. [6]. By applying a magnetic field gradient they made a system with a finite range of Zeeman fields. Phase diagram could be checked by observing the distribution of different spin components inside the trap (see figs 4.8, 4.9).

Another approach to studying the phase diagram of the ferromagnetic interactions in ^{87}Rb has been pursued by Sadler et. al. [7]. They started by preparing a condensate ground state in the large magnetic field and with net magnetization zero. This corresponds to a condensate of $m_F = 0$ state. Then

magnetic field was quickly lowered on the time scale that was too short for any dynamics of cold atoms to take place. Such experiments, where one or several parameters of the system are suddenly changed, are called *quench* experiments. After quenching the magnetic field Sadler et. al. had a system that was still a condensate of $m_F = 0$ atoms, although the microscopic Hamiltonian was already such that the system in the ground state should be a mixture of $m_F = \pm 1$ states. There are two ways to understand dynamics of the system following such quench. One approach is to calculate collective modes and observe that they have imaginary frequencies, indicating that the system is unstable towards exponential growth of fluctuations (see [18] and problem 4 in this Section). This is very similar to the analysis we did in the case of two component mixtures. By looking at the wavevector of the most unstable modes one can predict the size of domains. Another view on this dynamics is to observe that in the final state the system favors developing ferromagnetic order in the XY plane, i.e. spontaneous breaking of the symmetry of spin rotations around the z axis. On the other hand, initial state does not have any transverse magnetization. Initial state is fully symmetric with respect to U(1) rotations generated by F_z. Following the quench the system starts forming domains of transverse magnetization but magnetization directions differ in different points in space (see fig. 4.10). This leads to a state with random domains of transverse magnetization and the lengthscale of domains is set by the most unstable modes.

One possible extension of these types of experiments is to change the magnetic field at a finite rate, rather than suddenly. A general setting in which a continuous second order phase transition is crossed dynamically (but not instantaneously) from a state without symmetry breaking into a state with spontaneous symmetry breaking is often called Kibble-Zurek mechanism of domain formation. In such experiments one expects that a typical size of domains depends on the rate at which the transition is crossed. The faster is the crossing (less adiabatic), the smaller is the resulting domain size. A scaling argument predicts the relation between domain sizes and the rate[17]. Let H_c be the critical value of the magnetic field for which we expect a transition from the XY unordered to the XY ordered state, and let us define $g = H - H_c$. Second order transitions are characterized by the correlation length that should diverge at the transition $\xi \sim |g|^{-\nu}$. Dynamical critical exponent z relates lengthscales to timescales $\Delta \sim L^z \sim |g|^{z\nu}$. In our case $z = 1$ since in the easy plane ferromagnetic phase we have spin waves with linear dispertion. Energy scale Δ sets the gap to spin excitations in the disordered side and the energy of fluctuations of the magnitude of the order parameter on the broken symmetry side. As $H(t)$ is being changed, one can roughly separate adiabatic regime when $\dot{\Delta}/\Delta^2 << 1$ and antiadiabatic regime when $\dot{\Delta}/\Delta^2 >> 1$. To understand this condition think of the Lanadau-Zener problem or the problem of dynamically changing parameters of a harmonic oscillator. Far from the transition $\Delta(t)$ large, dynamics is adiabatic, i.e. the system can adjust itself to the changes of parameters. In the antiadiabatic regime, i.e. very close to the transition, the system can no longer follow changes in g. In this regime the system has very low energy modes, for which changes of the microscopic Hamiltonian are better treated as quenches.

So one can take a simplified perspective that in the entire antiadiabatic regime the wavefunction remains "frozen". Then the correlation length of the order parameter is simply the correlatin length ξ at the point when system dynamics changed from adiabatic to anti-adiabatic. For simplicity, let us consider $g = Ct$, where t is time, so that $\Delta(t) = \tilde{C}t^{z\nu}$. Transition from adiabatic to antiadiabatic regime takes place when $\tilde{C}^{-1}t_*^{-(z\nu+1)} \sim 1$. At the transition point $\xi_* \sim \tilde{C}^{-\frac{\nu}{z\nu+1}}$. This equation makes a prediction (not yet verified experimentally) for the domain size resulting from non-adiabatic crossing as a function of the rate of change of the magnetic field[17, 14] . It is worth mentioning that interesting analogies exist between questions of quench and Kibble-Zurek dynamics in cold atoms and problems of inflation and cosmology[11]. It is also possible to develop a more general theory that combines analysis of final state unstable modes and dynamics of changing microscopic parameters at a finite rate [14].

4.3 Beyond mean-field approximation

Let us now discuss the nature of S=1 ground states beyond the mean-field approximation. Let us assume that all particles are in a state of the lowest kinetic energy, but they can still have spin degrees of freedom. Taking the trap to be a box of size L^3 with periodic boundary conditions (this assumptions is not important and in a more realistic case L is replaced by the size of the ground state wavefunction), we can rewrite the Hamiltonian

$$\mathcal{H}_{\text{reduced}} = \frac{g_0}{2L^3}N^2 + \frac{g_s}{2L^3}\hat{\vec{F}}^2_{\text{tot}} \tag{4.13}$$

Here N is the total number of atoms and $\hat{\vec{F}}_{\text{tot}}$ is the operator of the total spin. There is a symmetry constraint that the allowed values of F_{tot} should have the same parity as the number of particles. This constraint arises from the condition that the spin part of the wavefunction must be symmetric under the exchange of any pair of atoms (the orbital part is symmetric since all atoms are assumed to be in the same orbital state).

When $g_s < 0$ the ground state has $F_{\text{tot}} = N$. This is the same ferromagnetic state we have seen in the mean-field analysis.

When $g_s > 0$ the ground state should have $F_{\text{tot}} = 0$ (assuming N is even). The question then arises how to reconcile this statement with the nematic state state obtained in the mean-field, which canbe written as $|\Psi_{\text{nem}}\rangle = \left(a^\dagger_{m_F=0}\right)^N |\text{vac}\rangle$. Again we need to appeal to spontaneous symmetry breaking. The state $|\Psi_{\text{nem}}\rangle$ does not have a well defined F_{tot}, so it is not a true eigenstate of the Hamiltoian and the direction of the nematic order should oscillate in time. The timescale of these oscillations is set by the difference of $F_{\text{tot}} = 0$ and $F_{\text{tot}} = 2$ eigenstates $T \sim \frac{\hbar}{\Delta E_{20}}$. From equation (4.13) we have

$$\Delta E_{20} = \frac{3g_s}{2L^3} = \frac{3g_s n}{N} \tag{4.14}$$

where $n = N/L^3$ is the density of particles. If we take thermodynamic limit while keeping $g_s n$ fixed (this is the energy scale proportional to the chemical potential $\mu = g_0 n$), we find that T becomes very long in the large N limit. Hence oscillations of the nematic order parameter can be neglected in this case. To observe the true spin single nature of the spin ground state with antiferromagnetic interactions, it is important to take mesoscopic systems, in which the number of particles is not too large.

4.4 Magnetic dipolar interactions

Magnetic dipolar interactions are given by

$$V_{\text{mag. dip}} = -\frac{\mu_0}{4\pi r_{12}^3}\left(3(\vec{m}_1\vec{e}_{12})(\vec{m}_2\vec{e}_{12}) - \vec{m}_1\vec{m}_2\right) \tag{4.15}$$

Here $\vec{e}_{12}$ is a unit vector parallel to the line joining the centers of the magnetic moments, r_{12} is the distance between the two moments, and $m_{1,2}$ are individual magnetic moments. We recall that contact interactions are given by $V_{\text{contact}} = (4\pi\hbar^2/m)\,\delta(r_1 - r_2)$. To understand the strength of dipolar interaction we take r_{12} to be of the order of a typical interatomic distance $n_0 r^3 \approx 1$. As an estimate of the strength of contact interaction we take chemical potential from equation (**??**). Then the ratio of the two interactions is given by

$$\epsilon \sim \frac{V_{\text{mag. dip}}}{V_{\text{contact}}} = \frac{\mu_0\mu^2 m}{12\pi\hbar^2 a_s} \tag{4.16}$$

Note that this ratio does not depend on the density. Typically $a_s \sim 100\,a_B$. For ^{87}Rb $\mu = \mu_B$ and $\epsilon = 0.007$. So dipolar interactions are less than one percent of the typical contact interactions. For ^{52}Cr $\mu = 6\mu_B$ and $\epsilon = 0.16$. Several beautiful experiments demonstrating magnetic dipolar interactions in Cr have been performed by T. Pfau's group (see [2, 10] for reviews).

It was argued magnetic dipolar interactions should be important for ^{87}Rb as well. It turns out that spin dependent part of the interaction is extremely small $a_2 - a_0 = -1.02a_B$. With spin dependent interactions being so weak, dipolar interactions become important in determining the spin structure of the condensate. Spontaneous formation of spin textures resulting from magnetic dipolar interactions have been reported by D. Stamper-Kurn's group [5, 9]. Later experiments by the same group, however, did not confirm these results.

It is also possible to switch off contact interact interactions using Feshbach resonance, then the only interaction term left will be magnetic dipolar interactions. This was explored in experiments in [8].

4.5 Spinor superfluids with higher spins

There are reasons to consider spinor superfluids with even larger spins. For example, both ^{87}Rb and ^{23}Na have $F = 2$ states, and ^{52}Cr atoms have $S =$

3. One of the difficulties of analyzing high spinor condensates is that many parameters needed to specify wavefunctions make their interpretation not very transparent. To specify the spin state of an $S = 1/2$ particle it is sufficient to specify direction of its spin (direction on the Bloch sphere). This fixes the wavefunction up to the overall phase factor. For $F = 1$ representation of the state in terms of the direction of the spin is applicable only for fully polarized states. A nematic state, such as $m_F = 0$ state, can not be represented by the direction of its spin polarization, since it has no expectation values of the spin operators. Majorana classification scheme, which we discuss in this section, is identifying states of spin F particles with $2F$ points on a sphere[1].

4.5.1 Majorana representation

Consider a particle of spin F in a state given by

$$|\psi\rangle = \sum_{m=-F}^{m=+F} A_m |m\rangle \tag{4.17}$$

Here A_m are a set of normalized complex coefficients and states $|m\rangle$ are eignestates of the F_z operator $F_z|m\rangle = m|m\rangle$. The idea is to find a set of maximally polarized states, which are orthogonal to $|\psi\rangle$. The maximally polarized state $|\zeta\rangle$ pointing in the direction $\vec{n} = (\theta, \phi)$ is determined by the equation $(\vec{n}\vec{F})\,|\zeta\rangle = F|\zeta\rangle$. A convenient (not normalized) representation of the polarized state $|\zeta\rangle$ is

$$\zeta\rangle = \sum_{\alpha=0}^{2F} \sqrt{\begin{pmatrix} 2F \\ \alpha \end{pmatrix}} \zeta^\alpha |F - \alpha\rangle \tag{4.18}$$

Here $\zeta = e^{i\phi}\tan(\frac{\theta}{2})$ is the stereographic mapping of the unit sphere to the complex plane. To understand equation (4.18) one can recall that state $|\zeta\rangle$ can be constructed by taking 2F spin 1/2 particles pointing in the direction $\vec{n}$ (experts in quantum magnetism can recognize the idea of Schwinger bosons here). Corresponding states of $S = 1/2$ particles are

$$|\zeta\rangle_{\frac{1}{2}} = e^{-i\phi/2}\cos\theta/2|\uparrow\rangle + e^{i\phi/2}\sin\theta/2|\downarrow\rangle \tag{4.19}$$

Writing a product of $2F$ of such states (symmetrization is automatic since we assume all bosons to be in precisely the same state)

$$|\zeta\rangle_{\frac{1}{2}} \ldots |\zeta\rangle_{\frac{1}{2}} = (e^{-i\phi/2}\cos\theta/2|\uparrow\rangle + e^{i\phi/2}\sin\theta/2|\downarrow\rangle)\ldots(e^{-i\phi/2}\cos\theta/2|\uparrow\rangle + e^{i\phi/2}\sin\theta/2|\downarrow\rangle) \tag{4.20}$$

in terms of the components of the total spin, we arrive at formula (4.18).

We define the characteristic polynomial for $|\psi\rangle$ in ζ to be

$$f_\psi(\zeta) = \langle\psi|\zeta\rangle = \sum_{\alpha=0}^{2F} \sqrt{\begin{pmatrix} 2F \\ \alpha \end{pmatrix}} A^*_{F-\alpha}\zeta^\alpha \tag{4.21}$$

The values of the 2F complex roots of $f_\psi(\zeta_i) = 0$, which are in correspondence with sets of points on the unit sphere, determine the coefficients A_m and therefore $|\psi\rangle$ up to normalization factor[1].

Majorana, representations of states of $F = 1$ atoms that we discussed before are shown in fig. 4.11. Majorana representations of possible states of $F = 2$ atoms are shown in fig. 4.13

4.5.2 $F = 2$ atoms

Phase diagram for $F = 2$ bosonic atoms is shown in fig. 4.12. Note that mean-field analysis is not sufficient to remove all degeneracies on the phase diagram. States of the form $(\frac{\sin\eta}{\sqrt{2}}, 0, \cos\eta, 0, \frac{\sin\eta}{\sqrt{2}})$ are degenerate at the mean-field level for any value of η. One needs to include fluctuations to understand the precise character of the nematic states[21]. Nonequilibrium spin dynamics of $F = 2$ states of ^{87}Rb atoms has been studied experimentally [19, 13] although the ground state properties have not been explored in experiments yet.

4.5.3 $F = 3$ atoms

Phase diagram for $F = 3$ bosonic atoms is shown in figs. 4.14, 4.15. Spin dynamics of S=3 ^{52}Cr atoms has been studied experimentally by Pasquuiou et al.[16]. Dipolar interactions are expected to play a major role in the dynamics of Cr atoms and complete understanding of these experiments is still lacking.

4.6 Problems for Chapter 4

Problem 1

Consider two component Bose mixture with the Hamiltonian (4.1). Assume all $U_{ij} > 0$. Derive $T = 0$ phase diagram as a function of $\mu_{\{1,2\}}$ in the mean-field approximation. Discuss relation to phase diagrams at fixed densities.

Problem 2

Starting with the two component linearized GP equations in (4.5), obtain the dispersion of colletive modes.

Problem 3

Consider F=1 spinor condensate with the Hamiltonian (4.10). Obtain the equilibrium phase diagrams as a function of p and q. Consider separately cases with $g_s < 0$ and $g_s > 0$.

Problem 4

Consider $F = 1$ spinor condensate with ferromagnetic interactions: $g_s < 0$ in (4.10). Assuming that all atoms are in the $m_F = 0$ state, calculate the spectrum of Bogoliubov excitations. Identify charge and spin modes. Discuss conditions for spin modes to have imaginary frequencies and compare to the equilibrium phase diagram. Such quench experiment has been done by Sadler et al. [7].

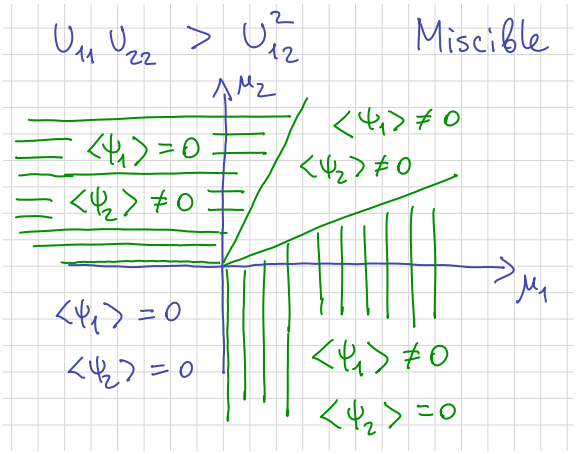

Figure 4.1: Phase diagram that corresponds to the miscible regime of two component Bose mixture.

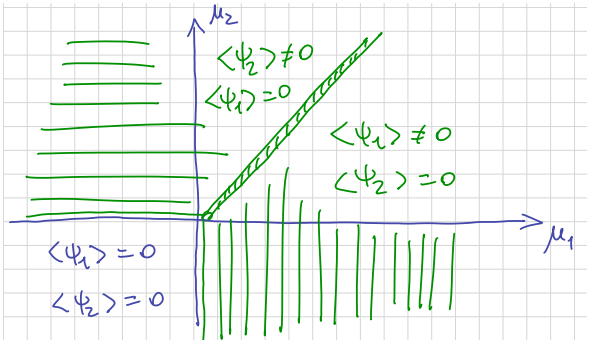

Figure 4.2: Phase diagram that corresponds to the immiscible regime of two component Bose mixture.

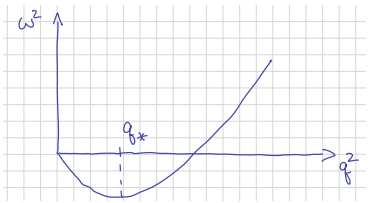

Figure 4.3: Collective modes for a two component uniform mixture in the immiscible regime. Negative values of ω^2 correspond to unstable modes. Dominant instability has the largest imaginary frequency and is marked with q_*.

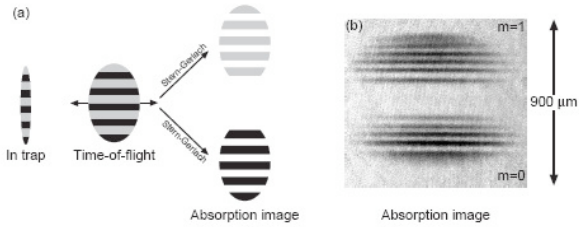

Figure 4.4: Spontaneous formation of spin domains. An overlapping $|m_F = 0, 1\rangle$ mixed condensate of Na was prepared at 15G. After about 50 ms domains started to form with a lengthscale of ≈ 40 μm. The $|m_F = 0\rangle$ and $|m_F = 1\rangle$ states were separated during the expansion for imaging. Fig. taken from [20].

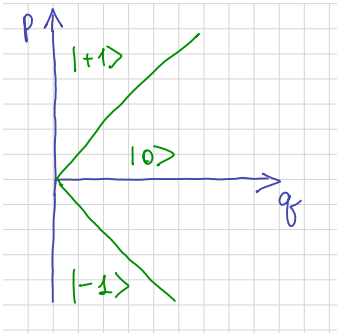

Figure 4.5: Phase diagram of $F = 1$ spinor condensates for $g_s = 0$.

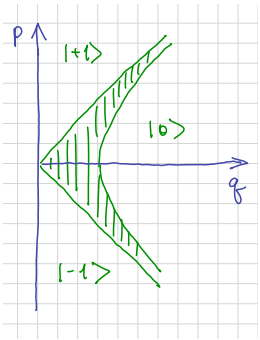

Figure 4.6: Phase diagram of $F = 1$ spinor condensates for *ferromagnetic* interactions, $g_s < 0$. Shaded regions are a mixture of all three states. There is a finite expectation value of the total spin in the XY plane.

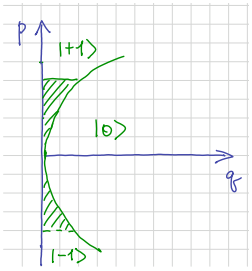

Figure 4.7: Phase diagram of $F = 1$ spinor condensates for *antiferromagnetic* interactions, $g_s > 0$. Shaded regions are a mixture of $|m_F = -1\rangle$ and $|m_F = +1\rangle$ atoms. Mixing $|m_F = \pm 1\rangle$ states lowers the interaction energy.

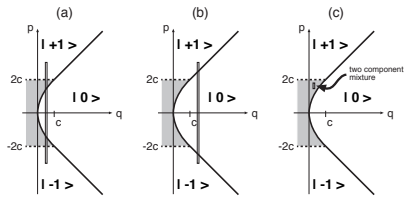

Figure 4.8: Using magnetic field gradient to explore the phase diagram of $F = 1$ spinor condensates with antiferromagnetic interactions, $g_s > 0$. The bar shows a range of Zeeman fields inside the trap due to magnetic field gradient. Distribution of different spin components measured experimentally for such systems is shown in fig. 4.9. Figure taken from [3].

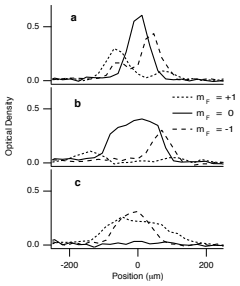

Figure 4.9: Experimental results corresponding to set-ups in fig. 4.8. Figure taken from [6]. Case a): Mixtures of states ± 1 are at the edges, state 0 is at the center of the trap. Case b): State $+1$ at one end, state -1 at the opposite end of the trap, state 0 in the center of the trap. Case c): Mixture of ± 1 states everywhere. Experimentally measured distributions of magnetic states are in qualitative agreement with the phase diagram in fig. 4.7.

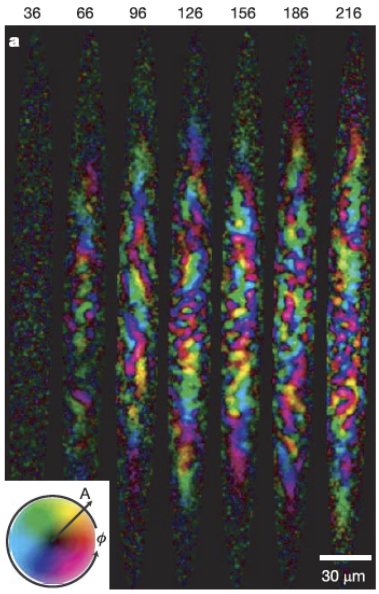

Figure 4.10: Magnetic domains in ferromagnetic $F = 1$ condensate resulting from sudden change of magnetic field from large H values to small ones. Figure taken from [7]. System develops transverse magnetization but orientations are not perfectly correlated. The same phenomenon can be analyzed by considering unstable collective modes[14, 18].

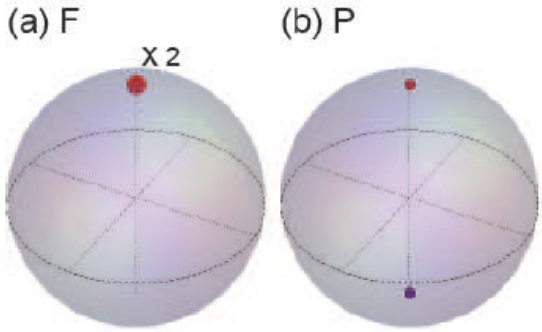

Figure 4.11: Majorana representation of states of $F = 1$ atom. Figure taken from [12]. Ferromagnetic state corresponds to a single doubly degenenerate point. Nematic (polar) state corresponds to two points at the opposite ends of a sphere.

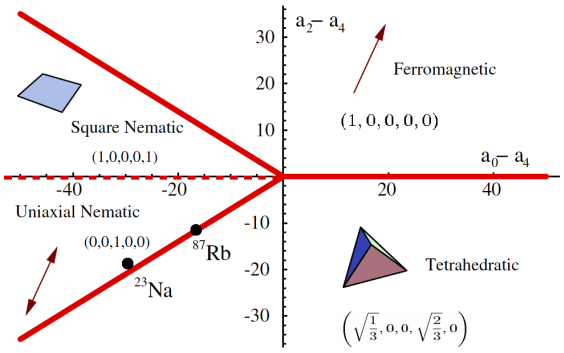

Figure 4.12: Phase diagram of $F = 2$ atoms from. Geometrical shapes describe Majorana repesentations of the appropriate states. Domains of stability of various nematic states were obtained by including energy of quantum fluctuations[21].

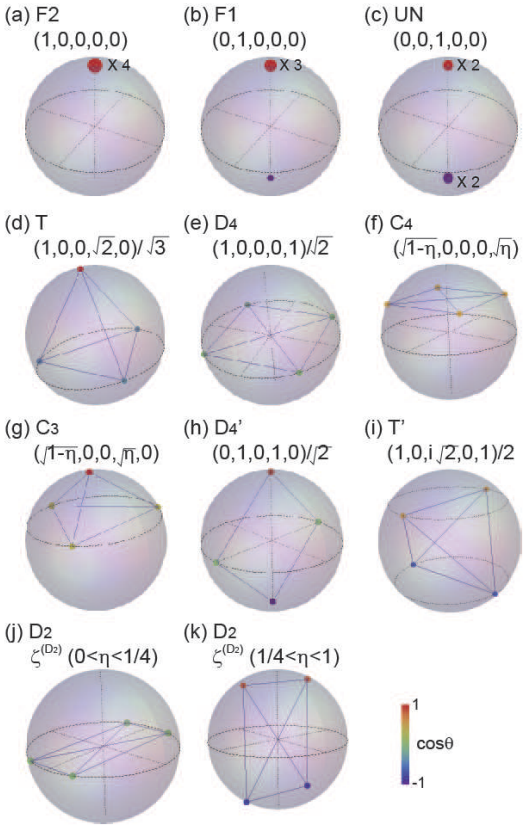

Figure 4.13: Majorana representation of states of several types of states $F = 2$ atom. Figure taken from [12]. Not all of these states shown here correspond to ground states for some choice of interaction constants. See fig. 4.12.

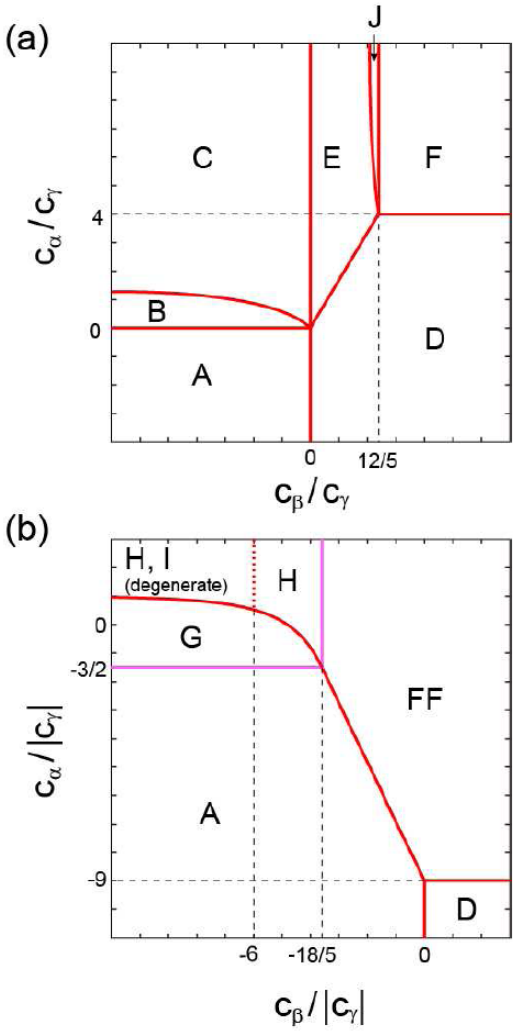

Figure 4.14: Phase diagram of $F = 3$ atoms from [12]. Here $C_\alpha = \frac{1}{7}(10a_6 - 21a_4 + 11a_0)$, $C_\beta = \frac{1}{7}(7a_6 - 18a_4 + 11a_2)$, and $C_\gamma = a_6 - a_4$. case a) corresponds to $C_\gamma > 0$ and case b) to $C_\gamma < 0$. Majorana repesentations of the appropriate states are given in fig4.15.

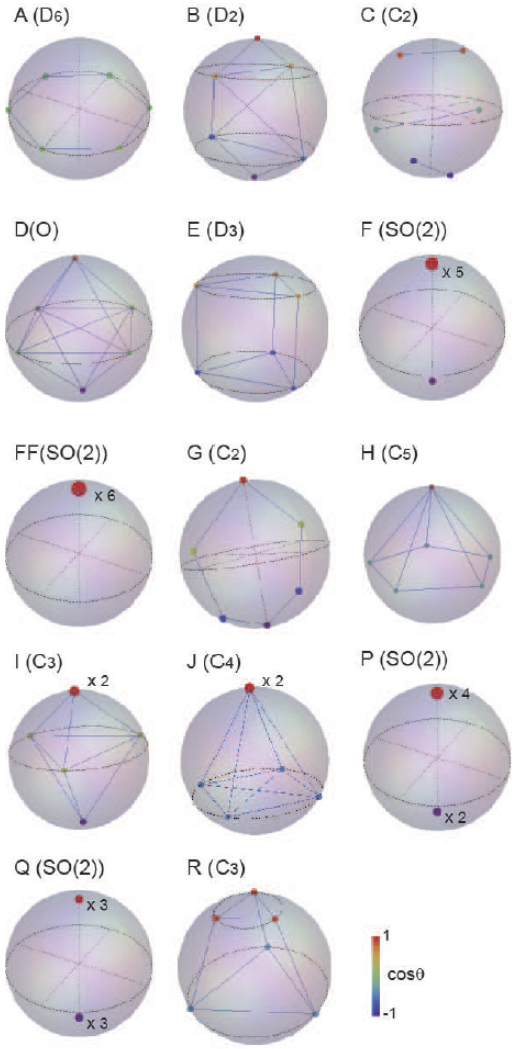

Figure 4.15: Majorana representation of states from the phase diagram 4.14. Figure taken from [12]. Note that all the states shown have some residual symmetry.

Bibliography

[1] Ryan Barnett, Ari Turner, and Eugene Demler. Classifying Novel Phases of Spinor Atoms. 180412(November):1–4, 2006.

[2] A. Griesmaier et al. *arXiv:cond-mat/0508423*, 2005.

[3] D. Stamper-Kurn et al. *Phys. Rev. Lett.*, 83:2876, 1999.

[4] H.J. Miesener et al. *Phys. Rev. Lett.*, 82:2228, 1999.

[5] H.J. Miesener et al. *Phys. Rev. Lett.*, 100:170403, 2008.

[6] J. Stenger et al. *Nature*, 396:345, 1998.

[7] L.E. Sadler et al. *Nature*, 443:312, 2006.

[8] M. Fattori et al. *Phys. Rev. Lett.*, 101:190405, 2008.

[9] M. Vengalattore et al. *arXiv:0901.3800*, 2009.

[10] T. Lahaye et al. *Rep. Prog. Phys.*, 72:126401, 2009.

[11] Vladimir Gritsev and Anatoli Polkovnikov. Universal Dynamics Near Quantum Critical Points. In *Developments in Quantum Phase Transitions*, pages 1–19.

[12] Yuki Kawaguchi and Masahito Ueda. Symmetry Classification of Spinor Bose-Einstein Condensates. pages 1–19, 2011.

[13] Jochen Kronjäger, Christoph Becker, Parvis Soltan-Panahi, Kai Bongs, and Klaus Sengstock. Spontaneous Pattern Formation in an Antiferromagnetic Quantum Gas. *Physical Review Letters*, 105(9):1–4, August 2010.

[14] Austen Lamacraft. Quantum Quenches in a Spinor Condensate. *Physical Review Letters*, 98(16):1–4, April 2007.

[15] Ao P. and Chui S.T. *J. Phys. B*, 33:535, 2000.

[16] B. Pasquiou, E. Maréchal, G. Bismut, P. Pedri, L. Vernac, O. Gorceix, and B. Laburthe-Tolra. Spontaneous Demagnetization of a Dipolar Spinor Bose Gas in an Ultralow Magnetic Field. *Physical Review Letters*, 106(25):1–4, June 2011.

[17] Anatoli Polkovnikov. Universal adiabatic dynamics in the vicinity of a quantum critical point. *Physical Review B*, 72(16):5–8, October 2005.

[18] Nicholas Robins, Weiping Zhang, Elena Ostrovskaya, and Yuri Kivshar. Modulational instability of spinor condensates. *Physical Review A*, 64(2):1–4, July 2001.

[19] H. Schmaljohann, M. Erhard, J. Kronjäger, M. Kottke, S. van Staa, L. Cacciapuoti, J. Arlt, K. Bongs, and K. Sengstock. Dynamics of F=2 Spinor Bose-Einstein Condensates. *Physical Review Letters*, 92(4):28–31, January 2004.

[20] D. Stamper-Kurn and W. Ketterle. *Proceedings of Les Houches 1999 Summer School, Session LXXII, arXiv:cond-mat/0005001*, 2000.

[21] Ari Turner, Ryan Barnett, Eugene Demler, and Ashvin Vishwanath. Nematic Order by Disorder in Spin-2 Bose-Einstein Condensates. *Physical Review Letters*, 98(19):1–4, May 2007.